Ground Penetrating Radar
The first peer-reviewed scientific journal dedicated to GPR

FALSE ALARM REDUCTION BY TARGET TRACKING FOR FORWARD LOOKING GROUND PENETRATING RADAR

YUKINORI FUSE[1], MASOUD ROSTAMI[1],
BORJA GONZALEZ-VALDES[2] & CAREY M. RAPPAPORT[1]

[1] DEPARTMENT OF ELECTRICAL AND COMPUTER ENGINEERING, NORTHEASTERN UNIVERSITY, BOSTON, MASSACHUSETTS, UNITED STATES OF AMERICA – YFUSE@ECE.NEU.EDU; MROSTAMI@ECE.NEU.EDU; RAPPAPORT@COE.NEU.EDU

[2] UNIVERSITY OF VIGO, VIGO, SPAIN – BGVALDES@COM.UVIGO.ES

ABSTRACT

An algorithm based on tracking stationary buried objects with advancing platform views is shown to reduce false alarms for Forward-Looking Ground Penetrating Radar (FLGPR). First, the Synthetic Aperture Radar (SAR) processed image is cleaned using a model-based clutter suppression method by applying masks to suppress the clutter signals. The mask is generated by L-band VV (vertical transmitting, vertical receiving), and VH (vertical transmitting, horizontal receiving) polarizations and X-band VV polarization SAR image results. Second, target tracking is applied to the clutter suppressed SAR image. These images are compared based on the system positions and the possible clutter signals are eliminated. The total detection performance is evaluated by a Receiver Operating Characteristic (ROC) curve with measurement data. The proposed method achieves significant reduction of the false alarm rate and improves the detection performance of the FLGPR system.

KEYWORDS: Imaging system; Synthetic Aperture Radar (SAR); Forward-Looking Ground Penetrating Radar (FLGPR).

1. INTRODUCTION

Buried explosive threats such as mines have been a problem for decades. Especially Improvised Explosive Devices (IEDs) are a significant problem and they are explosive devices assembled with conventional military weapon such as mines and projectiles and the detonating mechanism. Some types of sensors such as Ground Penetrating Radar (GPR), infrared sensor [1], acoustic sensor [2], and metal detector [3] have been studied and developed for a long time. Forward-Looking GPR (FLGPR) [4, 5] is also one of the approaches to

https://doi.org/10.26376/GPR2018012

detect these treats and with the advantages of a safe stand-off distance between the sensor vehicle platform and the buried threat, and wide area coverage. FLGPR must distinguish between target of interest and clutter, due to scattering from the rough ground surface, rocks, objects above the surface like trees, bushes, and more. Model-based clutter suppression method for FLGPR has been proposed to solve this problem.

In this work, a false alarm reduction method based on a target tracking with a model-based clutter suppression method is presented. The method is validated with a measurement data set provided by the United States (US) Army, Communications-Electronics Research, Development and Engineering Center (CERDEC), Night Vision and Electronic Sensors Directorate (NVESD). The FLGPR is a dual wideband radar system, which uses the lower frequency L-band (0.75~3.2 GHz) radar to sense subsurface objects, and the higher frequency X-band (8~12 GHz) radar to sense primarily the on-ground and above-ground scatterers. Model-based clutter suppression processing is able to clean the L-band Synthetic Aperture Radar (SAR) image using a mixture binary mask formed by L-band and X-band masks [6], with the binary mask covering just the clutter signals while excluding the buried target signals. The mask is applied to the L-band radar image and a new simulated response is generated. Primary clutter objects signals are subtracted from the original L-band signals, generating a clutter-suppressed SAR image with minimal reduction in buried target image intensity.

To reduce the false alarm rate further, a target tracking image processing method is proposed to supplement the model-based clutter suppression method. The tracking process is applied using SAR images at different Global Positioning System (GPS)-determined positions of the radar platform to track the buried target responses. This process is repeated for selected observation frames. Since grazing-incident refracted waves tend to be fairly independent of incident angle, underground objects tend to scatter similarly for most stand-off distances; and thus yield a consistent image, independent of platform position. This image consistency from the buried targets is a feature that is exploited to distinguish them from clutter objects.

https://doi.org/10.26376/GPR2018012

2. METHODOLOGY

This section explains the methodology of the false alarm reduction method. The system specification is described in Table I. The L-band radar has 8 transmitters and 8 receivers, and the X-band radar has 32 transmitters and 4 receivers. A GPS is mounted on the system so that the antenna positions are obtained at each system location. Therefore, reconstructed wideband array based images can be added together coherently with using multiple frames in the range direction to form the SAR image.

The target tracking method is applied after the model-based clutter suppression method [6]. Since the buried targets are static objects while the sensor system is moving forward, an estimated position can be derived from the position of the system at each observation frame. This position changes in the moving computational frame, corresponding to the movement of the vehicle between frames. The tracking procedure is divided into two main parts. The first part eliminates the possible false alarms by comparing the position of image peaks in different frames. In the second part, the tracking method is applied again to the positions declared in the first part to further eliminate false alarms. The procedure of the tracking method is described as:

[First part]

Step 1) Create the segments of the signals in a given image by choosing pixels above a certain threshold value in the current frame.
Step 2) Detect peaks of each segment in the image at the current frame number.
Step 3) Calculate the predicted position of each segment for the system positions from the next frames.
Step 4) Detect peaks of each segment in the next frame.
Step 5) Set the evaluation area based on the positions of Step 4 and compare to the estimated positions from Step 3.
Step 6) Decide and track using the results of Step 5.
Step 7) Repeat Steps 1 to 6, to identify additional possible targets.
Step 8) Declare the possible target positions in the first part.

https://doi.org/10.26376/GPR2018012

TABLE I – FLGPR SYSTEM.

	L-band radar	**X-band radar**
Antennas	8 transmitters, 8 receivers	32 transmitters, 4 receivers
Frequency bandwidth	0.75 GHz - 3.2 GHz	8.4GHz - 10.4 GHz

[Second part]

Step 9) Repeat Steps 1 to 8, discounting declared targets to track weaker signals and identify additional targets.

Step 10) Evaluate these results and declare the final target positions.

A series of images are used in this target tracking method to associate the positions of the peaks from frame to frame. The tracking method concept is presented in Figure 1, for $N + 1$ images. In this case, the front frame is frame #i and previous images from the past N platform positions have indexes from $i - N$ to #i. These can be used to estimate the position of the peak in the next frame image. The frame number "$i - N$" is the starting frame to obtain the result of frame #i. The SAR image is given by $I(x, y)$, and the peaks of the signals are calculated in the frame #$i - N$ as:

$$(p_{i-N}, q_{i-N}) = max[I_{i-N}(x, y)] \quad (1)$$

where (p_{i-N}, q_{i-N}) is the position within the regions at the front frame #$i - N$ of the image maximum. Since the vehicle mounted antenna platform is not necessarily moving in a straight line, it is important to re-register the images for every frame to ensure that the target responses from various frames overlap. The estimated position of the peaks can be calculated by the system position as:

$$p'_{i-N+1} = p_{i-N} - (X_{i-N+1} - X_{i-N}) \quad (2)$$

$$q'_{i-N+1} = q_{i-N} - (Y_{i-N+1} - Y_{i-N}) \quad (3)$$

where (p'_{i-N+1}, q'_{i-N+1}) is the estimated image maximum point of the region and (X_i, Y_i) is the i^{th} platform position. The next peak position in front frame #$i - N + 1$ is derived as:

https://doi.org/10.26376/GPR2018012

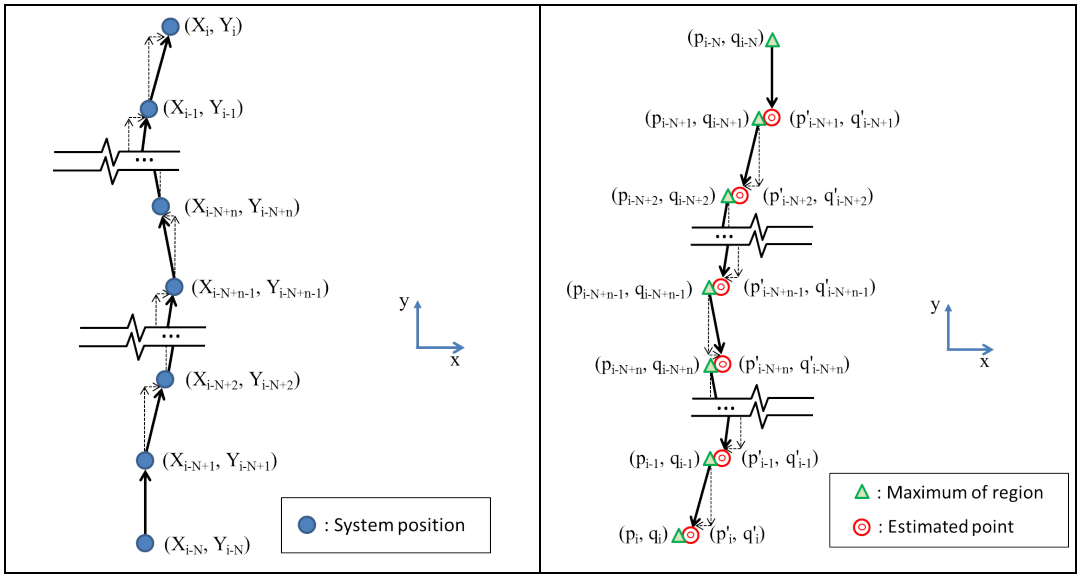

(a) **(b)**

FIG. 1 – Concept of the target tracking method: **(a)** System position in each frame. **(b)** Segment position in each frame.

$$(p_{i-N+1},\ q_{i-N+1}) = max\,[I_{i-N+1}\,(x,\ y)] \tag{4}$$

The comparison of the estimated position $(p'_{i-N+1},\ q'_{i-N+1})$ and (4) is made to decide whether the estimation position is sufficiently close; and if it is not close, that region is defined as clutter. This comparison is conducted for all discrete image maxima. The positions of the potential threats are used for calculating the next estimated position. The general estimation point in frame #n (n = 1, 2, ..., N) is presented as:

$$p'_{i-N+n} = p_{i-N+n+1} - (X_{i-N+n} - X_{i-N+n+1}) \tag{5}$$

$$q'_{i-N+n} = q_{i-N+n+1} - (Y_{i-N+n} - Y_{i-N+n+1}) \tag{6}$$

This procedure is repeated until the final comparison is made, $(p_i,\ q_i)$ and $(p'_i,\ q'_i)$. If the response persists for all frames, as shown in Figure 1(b), the region is declared a target candidate. A flowchart of this concept is given in Figure 2.

https://doi.org/10.26376/GPR2018012

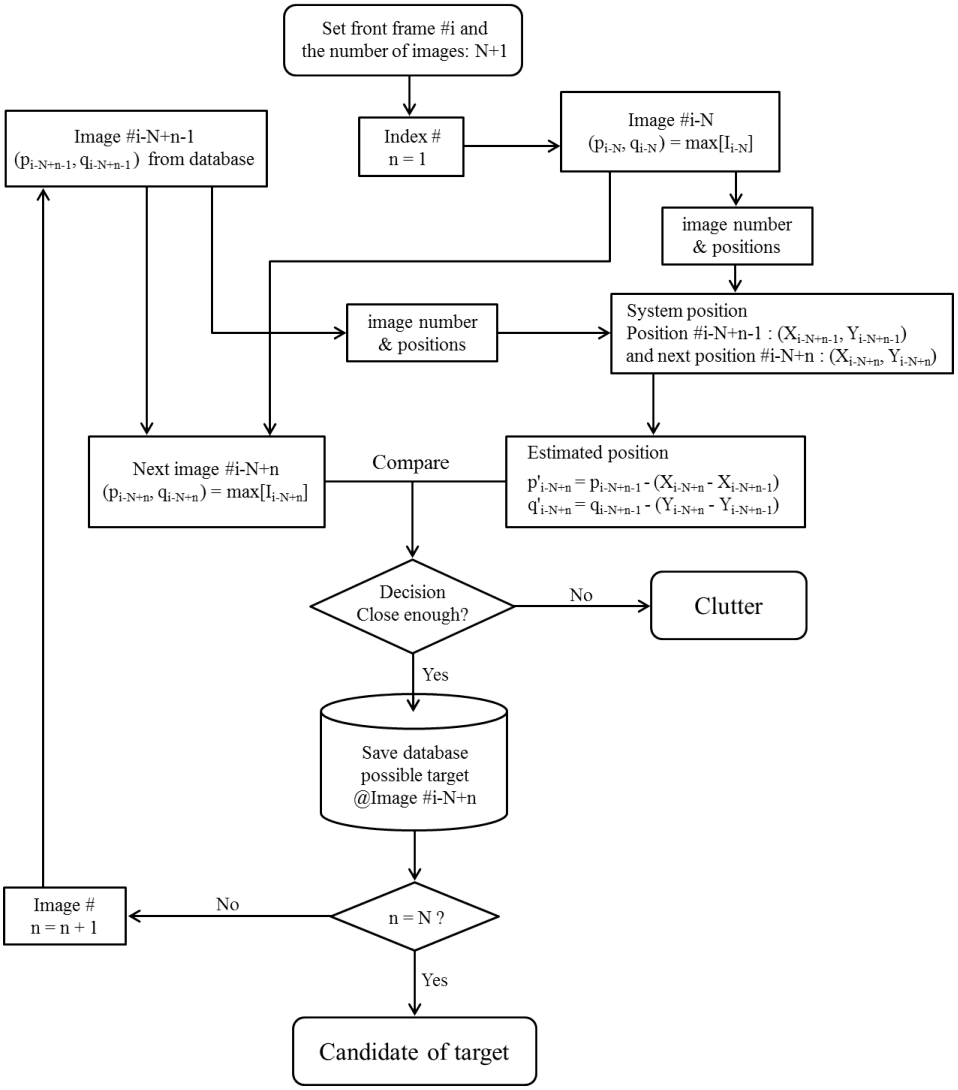

FIG. 2 – Flowchart of the target tracking method.

The second part of the method uses the same procedure as the first part, and it is applied to the output of the first part to further eliminate clutter signals. The positions of the possible target responses from the first part are compared to the positions of the vehicle, and if the responses are again declared, they have higher possibility of being target responses. Finally, the responses are declared as targets when they appear sequentially inside of the detection area. The parameters for the first and second parts are chosen from calibration runs in in the test lane.

https://doi.org/10.26376/GPR2018012

3. RESULTS

3.1 Pre-processing

An example of the original SAR image generated from field measured data is presented in Figure 3(a) [6], and the binary-mask clutter suppressed image is represented in Figure 3(b). Green triangle marker shows each true buried target (simulant explosives) position measured by GPS. In this paper, some buried targets are gathered in a group, but they are treated as one target. A noise reduction technique using a two-dimensional Gaussian smoothing filter [7] is applied to suppress small segments of the clutter signal in the image. Gaussian smoothing filters are widely used to reduce image noise and image details in digital image processing. The Gaussian filter is applied to the masking processed image scale in dB. An example of the pre-processing SAR image is shown in Figure 3(c). The Gaussian standard deviation parameter is selected as 0.8 to avoid eliminating the target signals. The number of segments in the masking processed image selected as non-target segments is 488, and the remaining number of non-target segments in the pre- processed image is 76. The potential false alarms are reduced by this pre-processing procedure.

3.2 First part of target tracking method

After applying image pre-processing, the peaks are considered as candidates for tracked responses. Examples of the pre-processed SAR image and the peak points are plotted with a black dot. As an example, for the first part of the tracking method, 28 sequential single frame step images are considered. Figure 4 represents the first comparison between images generated by the two approaches (Steps 1 - 6). The dot marks in Figure 4(a) are the peak points from the pre-processed image configuration. In Figure 4(b), the overlaid asterisk marks are the peak image points generated from the next antenna system position. The circle marks in Figure 4(c) are the peak positions of the next antenna positions. A test area is set based on the position of asterisk points, and when the pink circles are inside the test area, the positions are declared as target candidates. The evaluation area is arbitrarily set as 1.5 m wide in azimuth and 1.0 m in range. The red squares in Figure 4(d) show the declared positions. Comparing the predicted and newly-sensed images reduces some of the false alarms.

https://doi.org/10.26376/GPR2018012

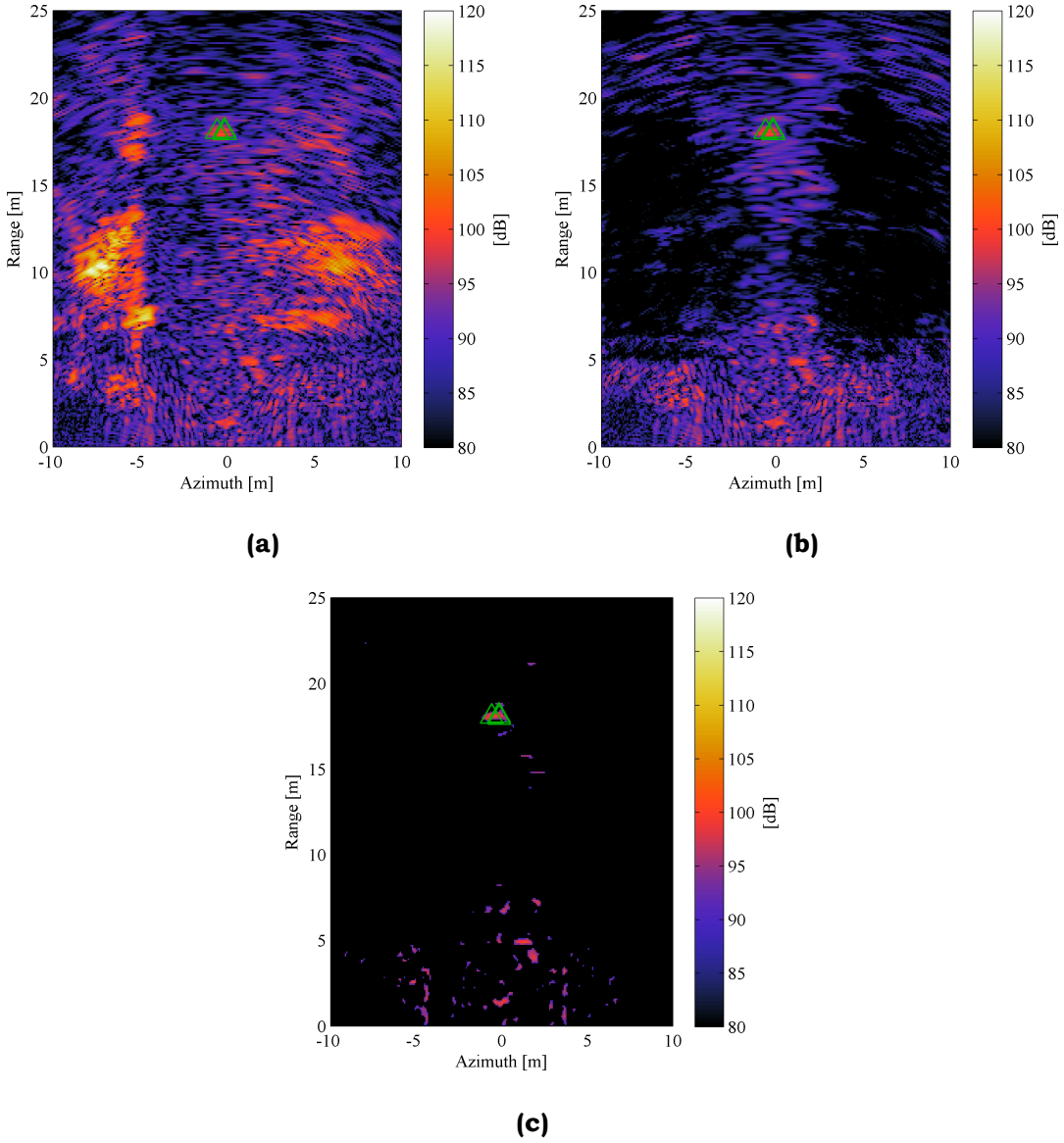

Fig. 3 – Model-based clutter suppression process image and pre-processed image. **(a)** Original SAR image. **(b)** Clutter suppression method SAR image. (c) Pre-processed SAR image. (Δ: True buried target position)

As an example, the procedure tested 28 images, with results presented in Figures 5–7. The declared points are plotted with white square boxes in the SAR image. After several iterations, the final declared potential target positions in the first step are shown in Figure 7. Figure 8 describes the relationship between the number of

https://doi.org/10.26376/GPR2018012

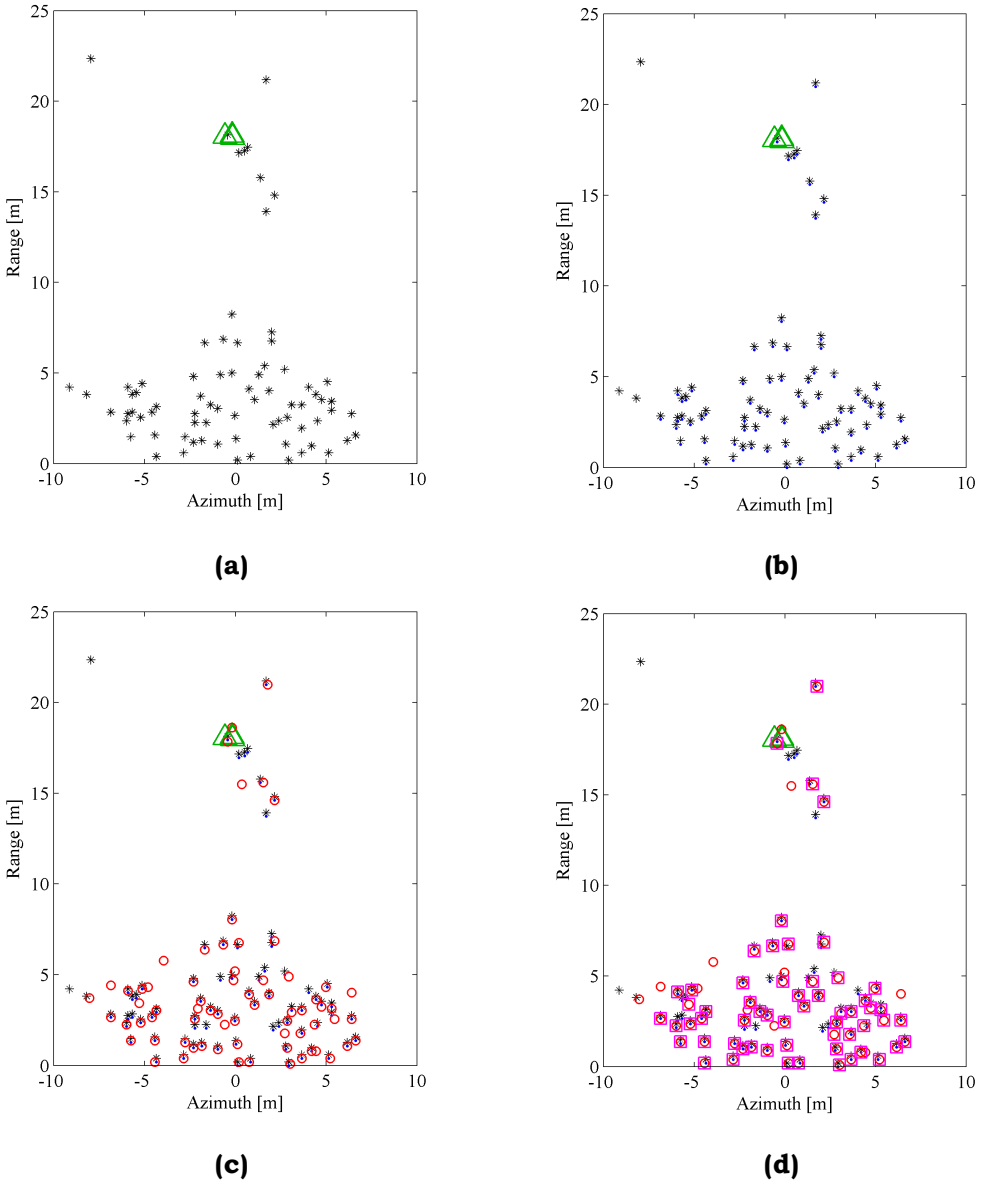

FIG. 4 – First part of the target tracking method, Steps 2-6. **(a)** Step 1. **(b)** Step 2. **(c)** Step 3. **(d)** Step 4 and 5. (· : Peak point in the current frame, ∗ : Estimated point of the next position, ◦ : Peak point in the next frame, □ : Declared point, Δ : True buried target position)

comparisons and the number of declared peaks. As presented in Figure 8, the number of declared peak points decreases by comparing the images frame by frame, from 77 at the 1st comparison to 7 at the 27th. The effectiveness of clutter reduction by the tracking method is confirmed.

https://doi.org/10.26376/GPR2018012

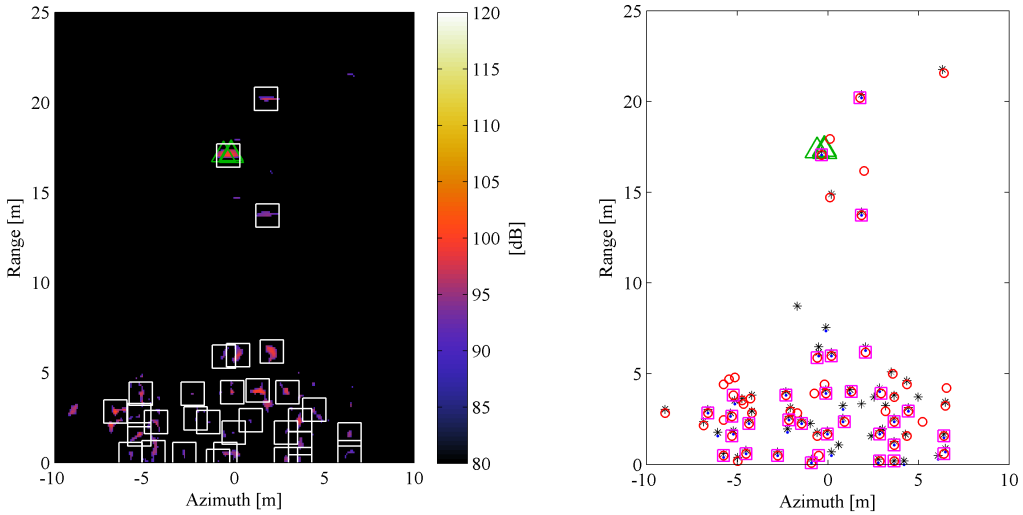

FIG. 5 – 5th comparison: **(a)** SAR image; **(b)** Peak plotted image. (∗ : Peak of current frame, · : prediction position, ◦ : Peak of next frame, □ : Declared point, Δ : True buried target position)

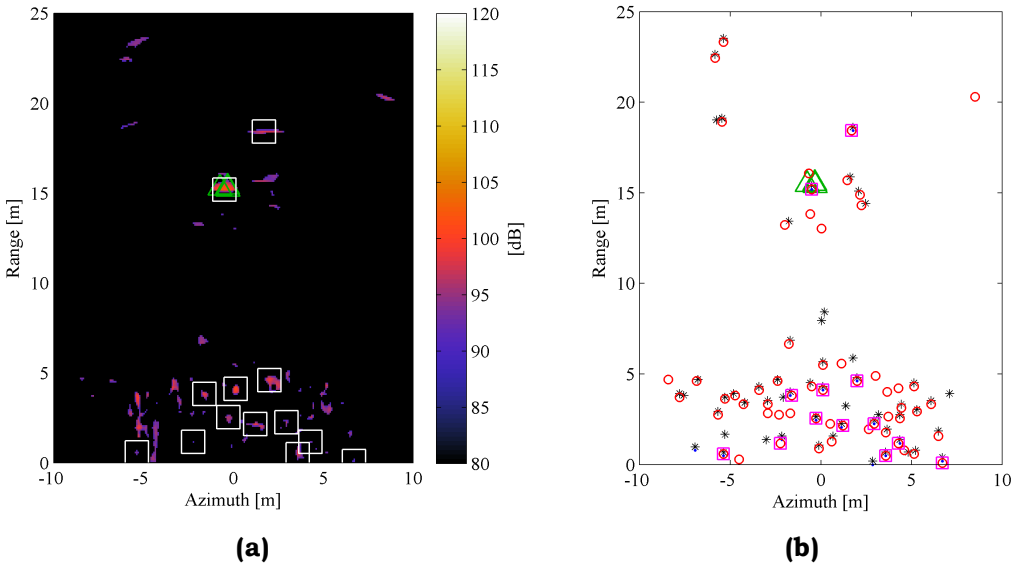

FIG. 6 – Same as in Fig. 5, 15th comparison.

https://doi.org/10.26376/GPR2018012

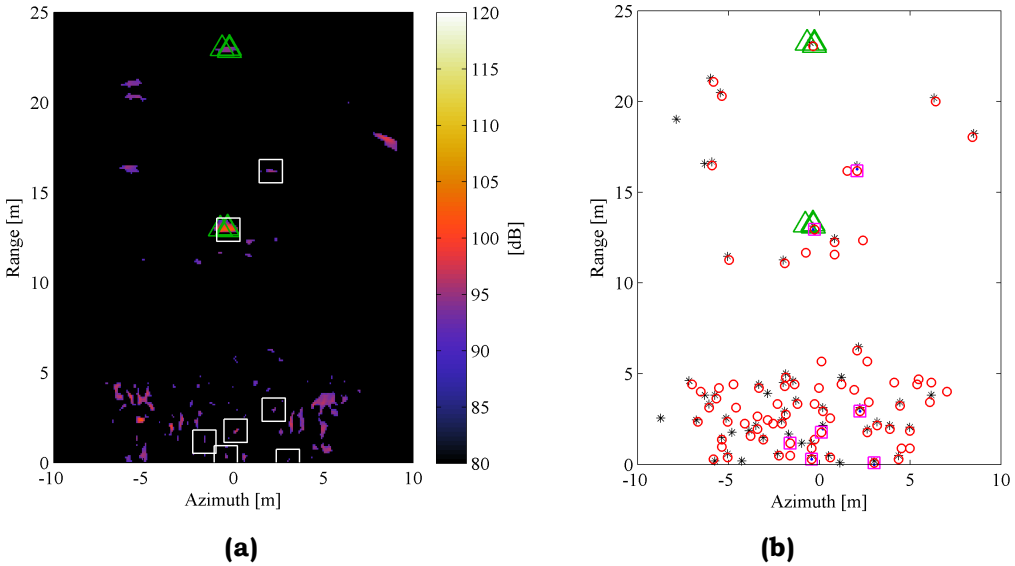

FIG. 7 – Same as in Fig. 5, 27th comparison.

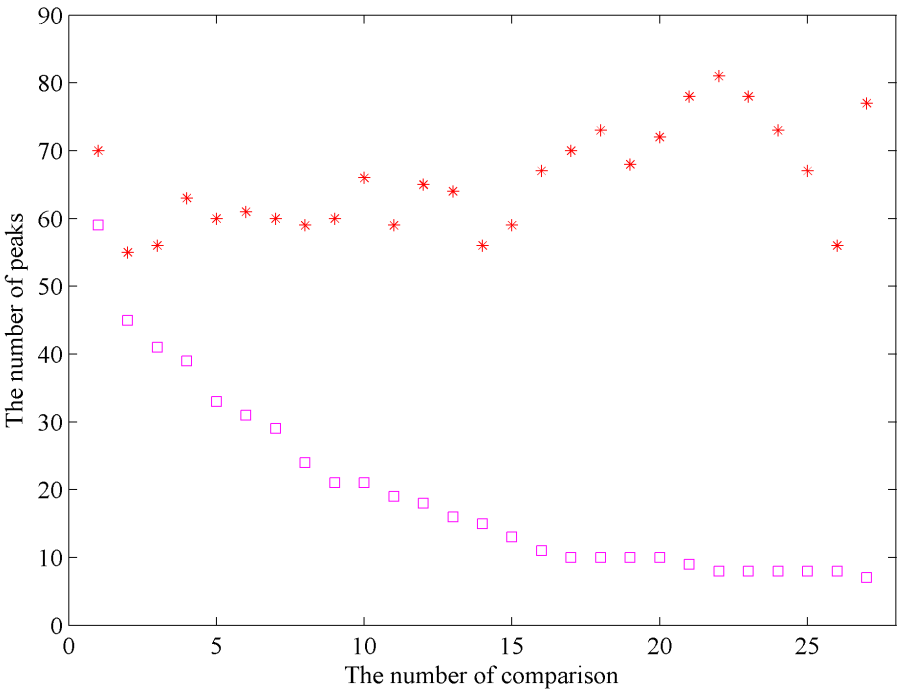

Fig. 8 – Relationship between the number of image comparison and the number of peaks (∗ : Peak point in the next frame, □ : Declared point)

https://doi.org/10.26376/GPR2018012

3.3 Second part of target tracking method

Second part of the target tracking method is based on the same concept as the first part. The positions of possible target responses from the first part are compared to the positions of the system, and if the signals are still declared, the responses have a higher probability of being target responses. Clutter responses are further eliminated, and the responses are confirmed as targets when the declared responses persist, appearing continuously within the detection area. Example results are presented in Figures 9–12. Each figure contains the results of the original SAR, the model-based clutter suppression processed image, and the target tracking processed image.

The potential target locations from the first part of the target tracking method are indicated with white markers, which are tracked during the second part of target tracking.

When a white marker appears continuously 7 times inside of the detection area, it is converted into a green marker, which indicates a higher probability of it being a target. An identification number is associated with each green square marker. When a green marker appears more than 3 times inside the detection area, it is changed into a square magenta marker and declared as a detected target. For example, the marker ID number 1 is located inside of the detection area, the green marker shown in Figure 11 is changed into the magenta marker as shown in Figure 12. This procedure is repeated continuously in every forward moving frame. The detection area for this particular sensing application is set as -7 m to 7 m in azimuth limit and 5 m to 10 m in range. The target is tracked simply and is effectively declared as detected by comparing the masking processed SAR images for various system positions.

4. Evaluations

The FLGPR target tracking method was extensively tested for multiple targets and a large variety of clutter on two lanes, lane A and lane B. In the test lanes, the buried targets were metal objects with different burial depths. Receiver Operating Characteristics (ROC) curves are used to evaluate the detection performance of the system, presenting the relationship between the probability detection (Pd) and the False Alarm Rate (FAR). FAR is calculated as the total number of false alarms per

https://doi.org/10.26376/GPR2018012

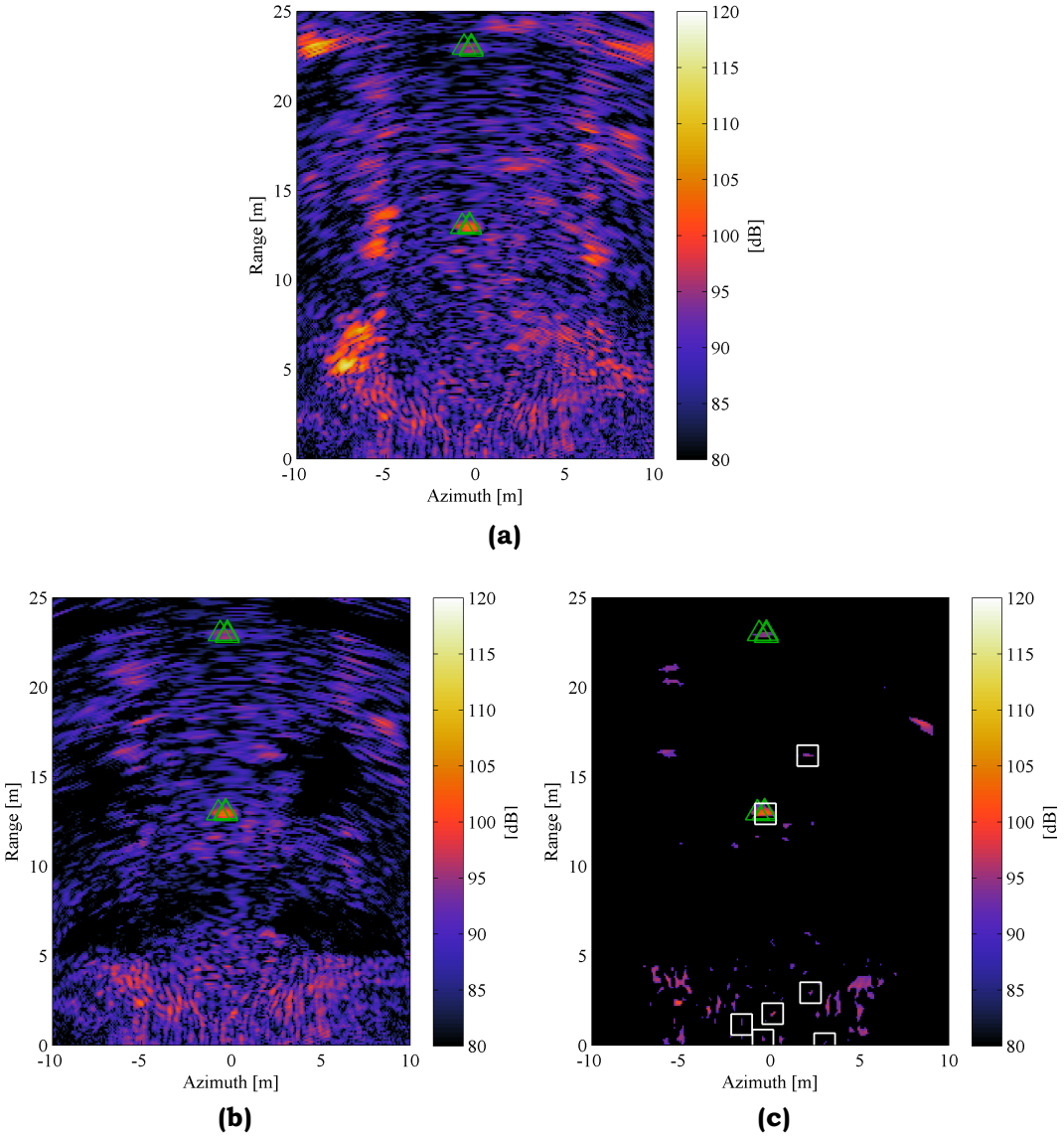

FIG. 9 – Second part of the target tracking method: Step 9 (1st output in second part): **(a)** Original SAR image; **(b)** Model-based clutter suppression SAR image; **(c)** Target tracking processed SAR image. (Δ: True buried target position, White square: First part tracked position).

the total sensing area, which is the accumulated detection area for all measured frames. The detection area is -7 m to 7 m in azimuth and 5 m to 10 m in range. The halo area for evaluation of the detected target is derived from the location of the ground truth target, with a diameter of 1 m. When a signal that rises above a specified threshold is located

https://doi.org/10.26376/GPR2018012

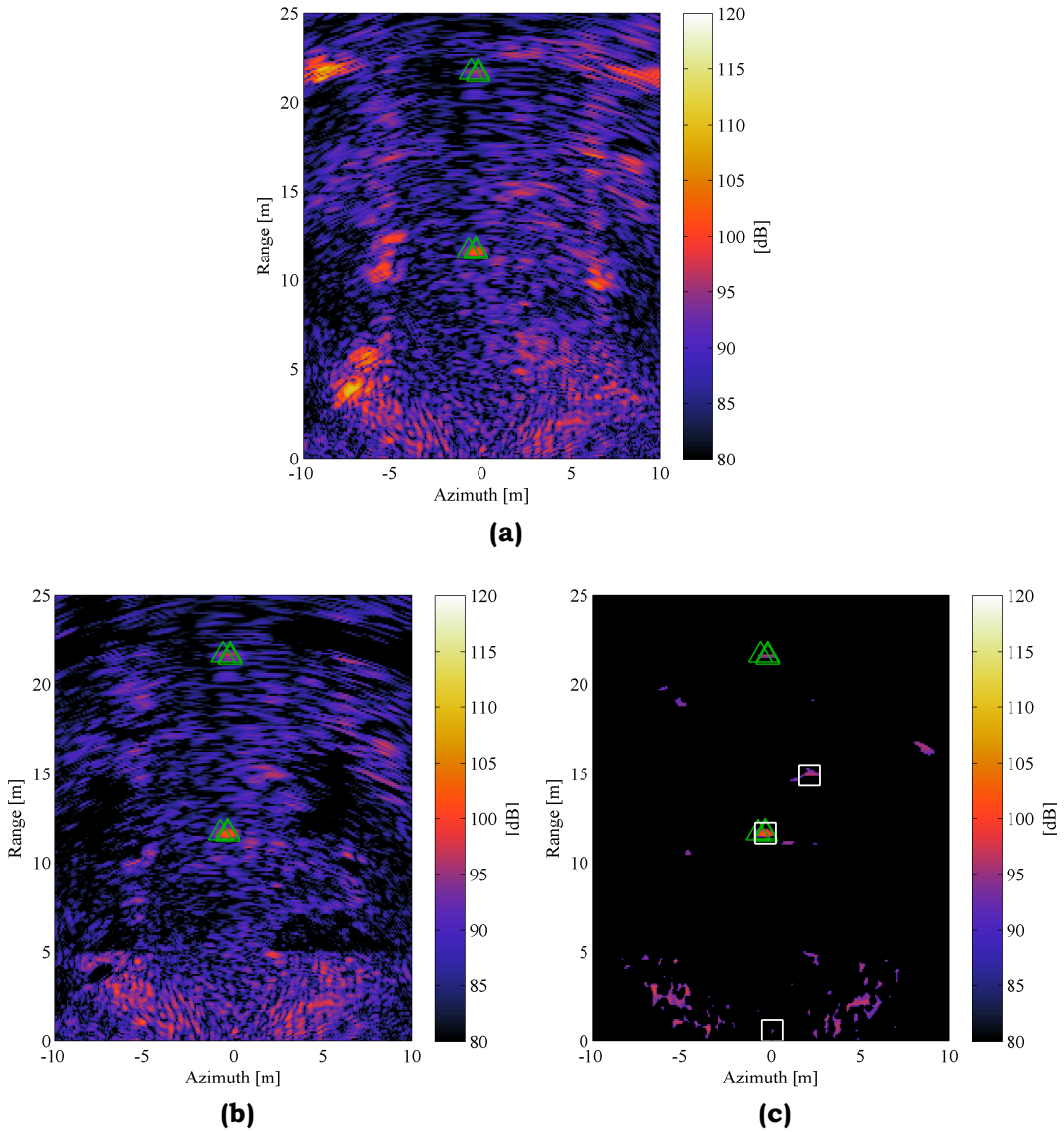

FIG. 10 – Same as in Fig. 9, for the 7th output in second part.

inside the halo, the signal is scored as a detected target. The resulting ROC in lanes A and B are presented in Figures 12 and 13. These figures present the detection results for the original SAR image, the model-based clutter suppression processed SAR image, and the target tracking processed image. Figures 12(b) and 13(b) show the performance details for target tracking. Based on these figures, the false alarm rate is reduced by almost 50 times using the proposed tracking method.

https://doi.org/10.26376/GPR2018012

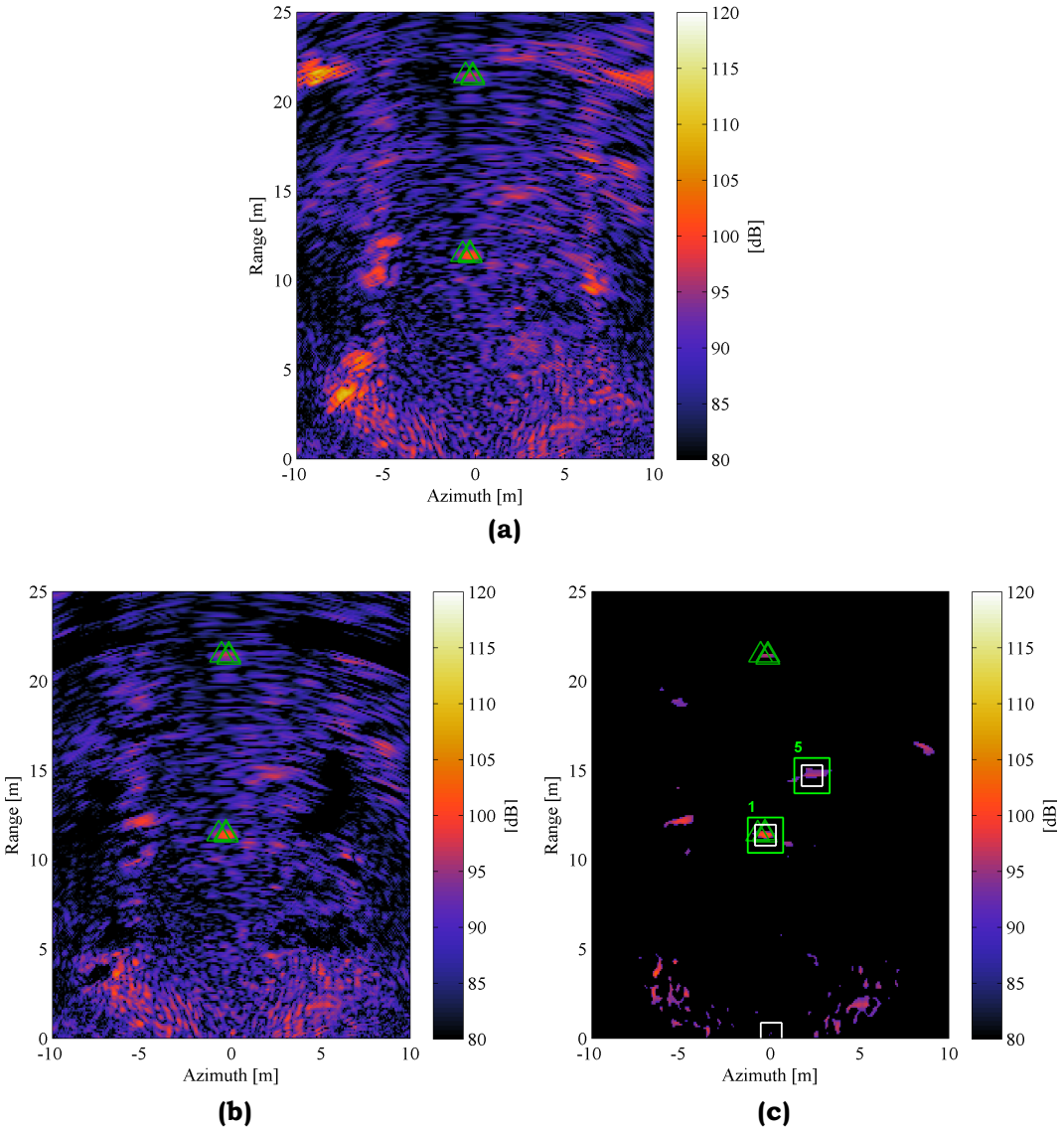

FIG. 11 – Same as in Fig. 9, for the 8th output in second part. Green squares represent the second part tracked position.

5. CONCLUSION

An advanced model-based target tracking clutter suppression process for the dual-band FLGPR was presented. The proposed method tracks and identifies buried targets by comparing the system position frame by frame and eliminating the more rapidly varying clutter images. The clutter suppression has been applied to the two lane data sets, and the

https://doi.org/10.26376/GPR2018012

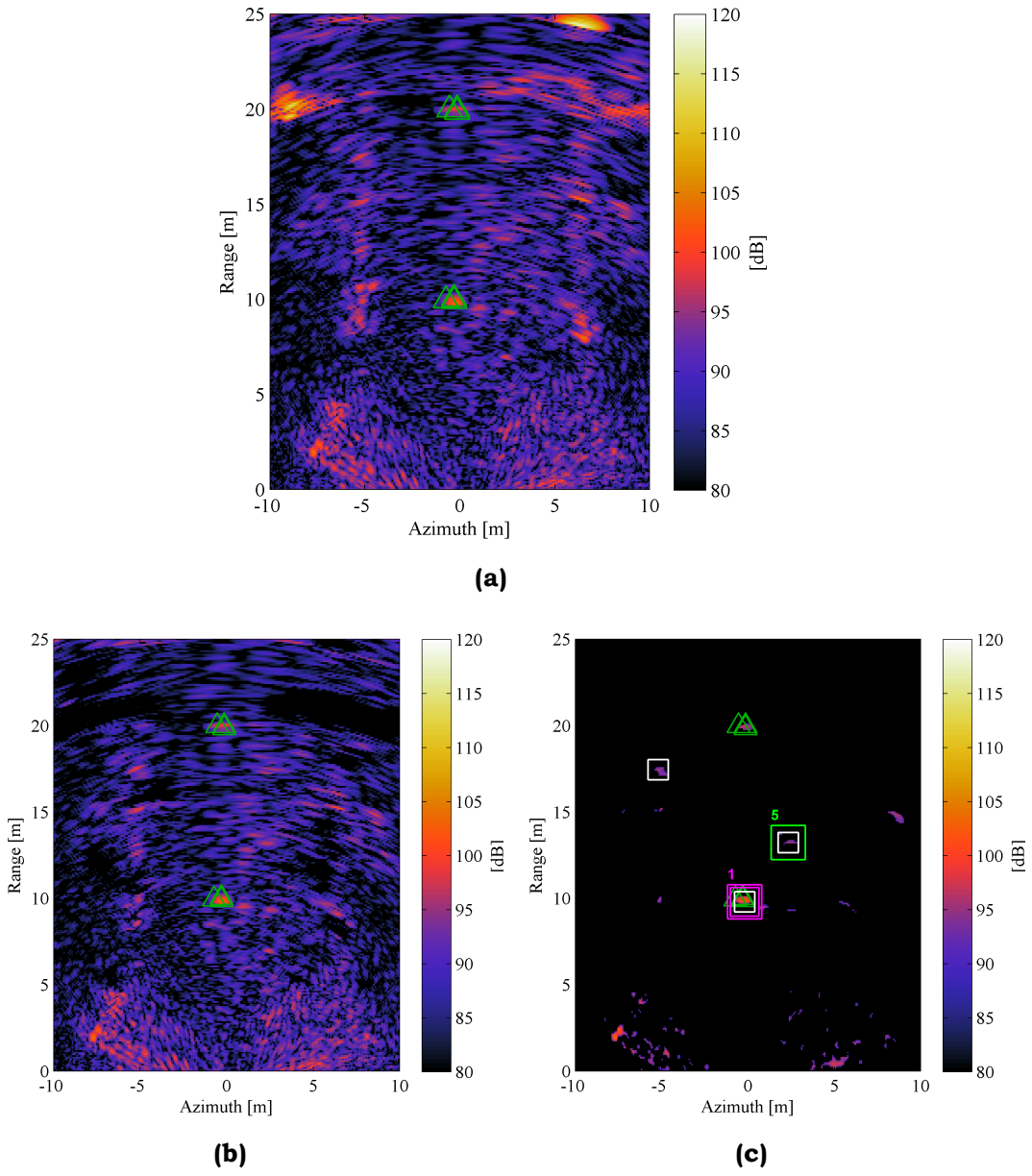

FIG. 12 – Second part of the target tracking method: Step 10 (15th output in second part): (a) Original SAR image; (b) Model-based clutter suppression SAR image; (c) Target tracking processed SAR image. (Δ: True buried target position, White square: First part tracked position, Green square: Second part tracked position, Magenta square: Detected target position).

https://doi.org/10.26376/GPR2018012

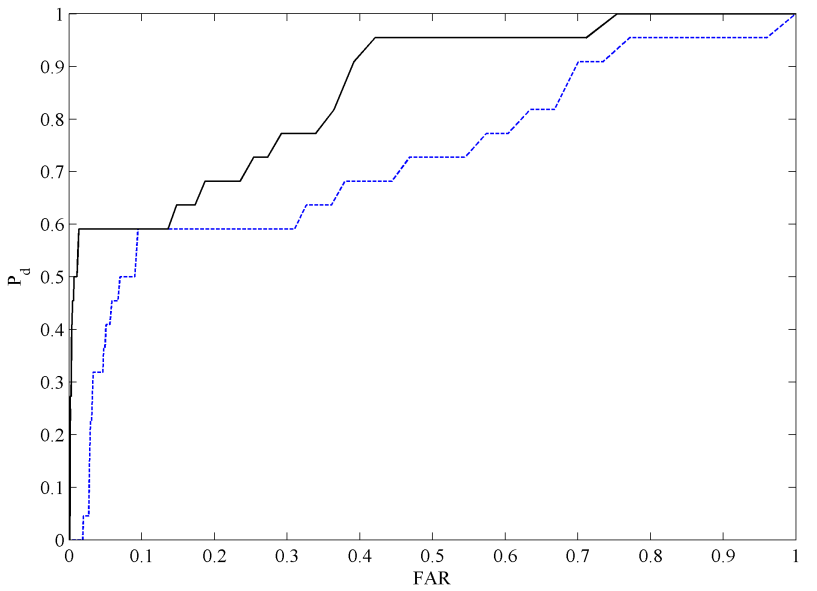

(a)

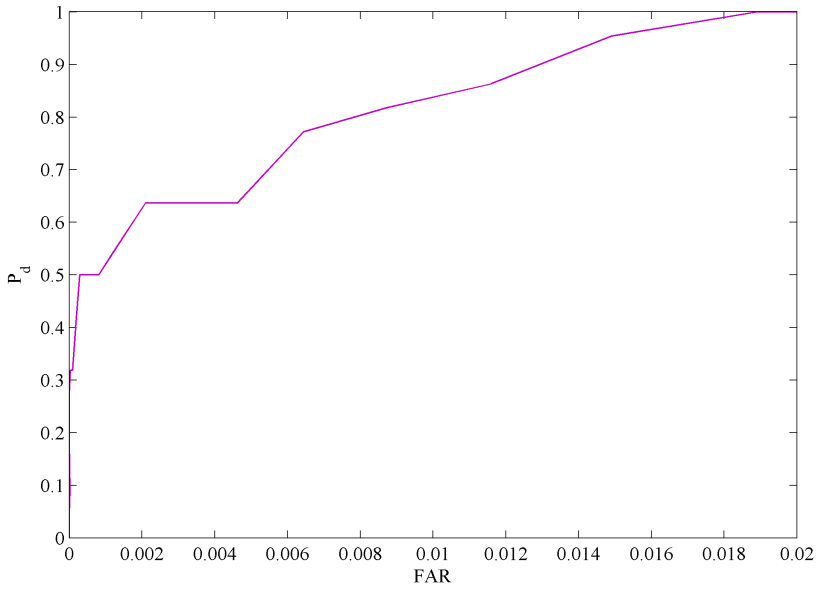

(b)

FIG. 13 – ROC curve of lane A with metal target: **(a)** No target tracking applied (--------: Original SAR image, ———: Model-based clutter suppression processed image); **(b)** With target tracking (note expanded FAR scale).

https://doi.org/10.26376/GPR2018012

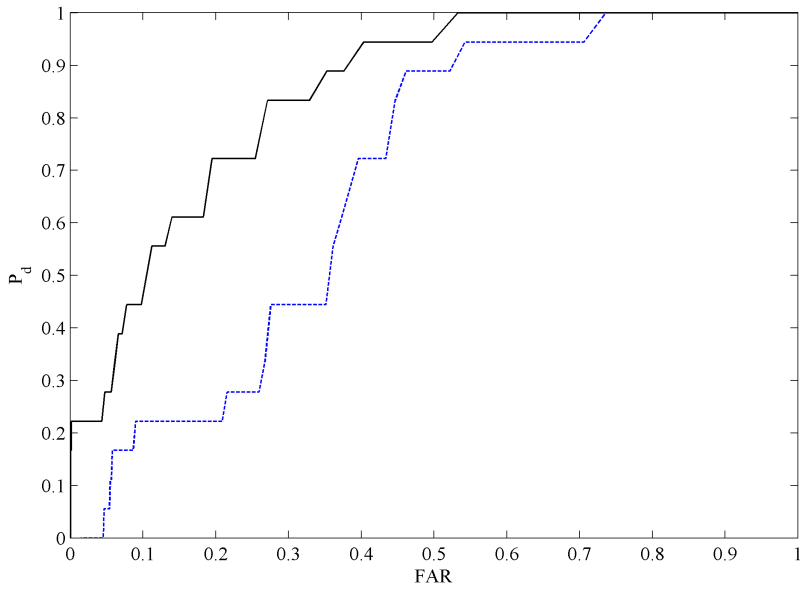

(a)

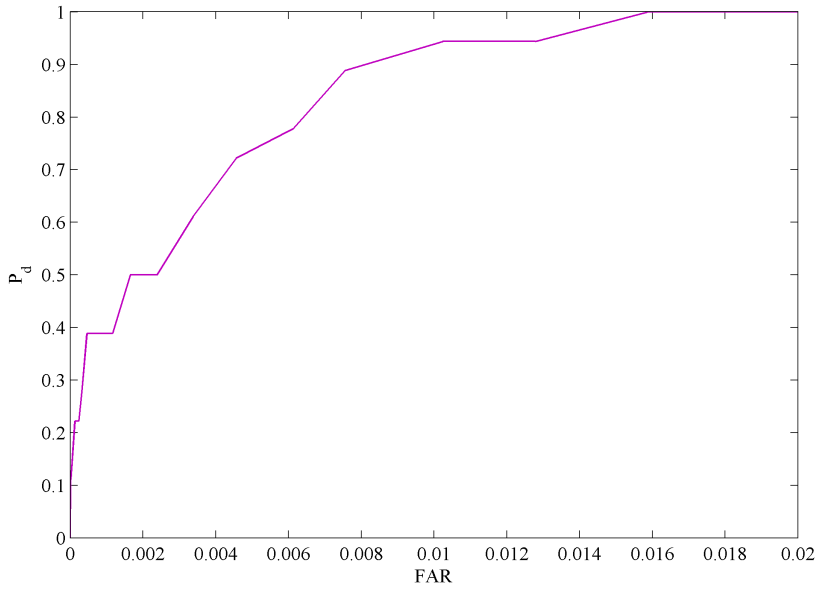

(b)

FIG. 14 – Same as in Fig. 13, for lane B.

https://doi.org/10.26376/GPR2018012

detection performance has been evaluated by using the ROC. One of the lanes is used as the test lane for optimizing the system threshold parameters and the other was used to test the algorithm. The result of test lane measurements also shows that the presented clutter reduction method is able to significantly improve the false alarm rate.

Ackwnowledgement

This work is supported by the U.S. Army CERDEC NVESD (W909MY12C0028).

References

[1] N. Playle, D. M. Port, R. Rutherford, I. A. Burch, and R. Almond, "Infrared polarization sensor for forward-looking mine detection," 2002 AeroSense conference of the International Society for Optics and Photonics, Orlando, FL, US – Proceedings of the SPIE, vol. 4742: Detection and Remediation Technologies for Mines and Minelike Targets VII, August 2002, pp. 11–18, doi: 10.1117/12.479086.

[2] B. J. Copenhaver, J. D. Gorhum, C. M. Slack, M. L. Barlett, T. G. Muir, and M. F. Hamilton, "Acoustic response of a buried landmine with a low grazing-angle source array, focused on the ground," Proceedings of Meetings on Acoustics, Acoustical Society of America, vol. 19, no. 1, 2 June 2013, Montreal, Canada, Article ID 045067, 6 pp., doi: 10.1121/1.4799604.

[3] M. Sato, J. Fujiwara, X. Feng, Z.-S. Zhou, and T. Kobayashi, "Development of a hand-held GPR MD sensor system (ALIS)," 2005 Defense and Security conference of the International Society for Optics and Photonics, Orlando, FL, US – Proceedings of the SPIE, vol. 5794: Detection and Remediation Technologies for Mines and Minelike Targets X, June 2005, pp. 1000–1007, doi: 10.1117/12.603213.

[4] L. Nguyen, "Signal and image processing algorithms for the US Army Research Laboratory: Ultra-wideband (UWB) Synchronous Impulse Reconstruction (SIRE) radar," Defence Technical Information Center (DTIC), Technical Report ARL-TR-4784, April 2009, 68 pp.

[5] K. Stone, J. Keller, K. Ho, M. Busch, and P. Gader, "On the registration of FLGPR and IR data for a forward-looking landmine detection system and its use in eliminating FLGPR false alarms," Proceedings of the Defense and Security Symposium of the International Society for Optics and Photonics – Proceedings of the SPIE, vol. 6953: Detection and Sensing of Mines, Explosive Objects, and Obscured Targets XIII, April 2008, Article ID 695314, 12 pp., doi: 10.1117/12.782238.

https://doi.org/10.26376/GPR2018012

[6] Y. Fuse, B. Gonzalez-Valdes, J. A. Martinez-Lorenzo, and C. M. Rappaport, “Advanced SAR imaging methods for forward-looking ground penetrating radar,” Proceedings of the 10th European Conference on Antennas and Propagation (EuCAP 2016), Davos, Switzerland, 10–15 April 2016, pp. 1–4, doi: 10.1109/EuCAP.2016.7481192.

[7] R. Jain, R. Kasturi, and B. G. Schunck. “Machine vision,” Publishing House: McGraw-Hill, Inc.; Book Series: “Computer Science;” New York, 1 May 2008; ISBN-13: 978-0070320185; ISBN-10: 0070320187; 549 pp.

https://doi.org/10.26376/GPR2018012

The scientific paper that you have downloaded is included in Issue 2, Volume 1 (July 2018) of the journal *Ground Penetrating Radar* (ISSN 2533-3100; journal homepage: www.gpradar.eu/journal).
All *Ground Penetrating Radar* papers are processed and published in true open access, free to both Authors and Readers, thanks to the generous support of TU1208 GPR Association and to the voluntary efforts of the journal Editorial Board. The publication of Issue 2, Volume 1 is also supported by Adapis Georadar Teknik Ab (georadar.eu) and by IDS Georadar s.r.l. (idsgeoradar.com).
The present information sheet is obviously not part of the scientific paper.